© 2021. Published by The Company of Biologists Ltd | Journal of Cell Science (2021) 134, jcs254011. doi:10.1242/jcs.254011

RESEARCH ARTICLE

Twinfilin1 controls lamellipodial protrusive activity and actin turnover during vertebrate gastrulation

Caitlin C. Devitt[1], Chanjae Lee[1], Rachael M. Cox[1], Ophelia Papoulas[1], José Alvarado[2], Shashank Shekhar[3,4], Edward M. Marcotte[1] and John B. Wallingford[1,*]

ABSTRACT

The dynamic control of the actin cytoskeleton is a key aspect of essentially all animal cell movements. Experiments in single migrating cells and *in vitro* systems have provided an exceptionally deep understanding of actin dynamics. However, we still know relatively little of how these systems are tuned in cell-type-specific ways, for example in the context of collective cell movements that sculpt the early embryo. Here, we provide an analysis of the actin-severing and depolymerization machinery during vertebrate gastrulation, with a focus on Twinfilin1 (Twf1) in *Xenopus*. We find that Twf1 is essential for convergent extension, and loss of Twf1 results in a disruption of lamellipodial dynamics and polarity. Moreover, Twf1 loss results in a failure to assemble polarized cytoplasmic actin cables, which are essential for convergent extension. These data provide an *in vivo* complement to our more-extensive understanding of Twf1 action *in vitro* and provide new links between the core machinery of actin regulation and the specialized cell behaviors of embryonic morphogenesis.

KEY WORDS: Actin, Cofilin, Convergent extension, Gastrulation, Twinfilin, Lamellipodia

INTRODUCTION

Convergent extension (CE) is an evolutionarily conserved collective cell movement in which a group of cells iteratively intercalate along a single axis, thus elongating the tissue in the perpendicular axis (Fig. 1A). CE drives the elongation of the body axis in essentially all animals and is critical for the shaping of diverse organs, including the kidney, heart and cochlea, so defects in CE are directly implicated in human congenital anomalies, including neural tube closure defects and limb differences (Huebner and Wallingford, 2018; Shindo, 2018; Tada and Heisenberg, 2012; Wallingford et al., 2002). Despite its importance in development and disease, CE has received far less attention than other types of cell motility. Indeed, while the integration of actin assembly and disassembly, actomyosin contraction, and cell adhesion have been exhaustively defined in single migrating cells (e.g. Devreotes et al., 2017; Gardel et al., 2010; Lawson and Ridley, 2018), such systems remain only rudimentarily described in CE.

[1]Department of Molecular Biosciences, University of Texas, Austin, TX 78712, USA. [2]Department of Physics, University of Texas, Austin, TX 78712, USA. [3]Department of Physics, Emory University, Atlanta, GA 30322, USA. [4]Department of Cell Biology, Emory University, Atlanta, GA 30322, USA.

*Author for correspondence (Wallingford@austin.utexas.edu)

S.S., 0000-0003-1494-0151; J.B.W., 0000-0001-8701-4293

Handling Editor: Andrew Ewald
Received 10 September 2020; Accepted 12 May 2021

An especially intriguing question relates to actin assembly and turnover, two aspects of lamellipodial action that have been particularly well studied in migrating cells *in vitro* but have not been studied during CE. In single cells, actin filaments are polymerized at the leading edge by the interaction of membrane-bound proteins, actin regulators, actin monomers and existing actin filaments. As actin monomers are added to the distal end, existing filaments push on the plasma membrane, displacing the filaments towards the cell-proximal portion of the lamellipodia in a process termed retrograde flow (Gardel et al., 2010; Theriot and Mitchison, 1991). At the rear (cell proximal side) of the lamellipodia, the lamella, focal adhesions attach actin fibers to the substrate or an extracellular matrix. Here, lamellipodial actin filaments are disassembled through filament severing and/or depolymerization (Carlier et al., 2015; Rottner and Schaks, 2019; Shekhar and Carlier, 2017). The roles of actin regulatory proteins in migration of single cells have been documented extensively, including those of actin assembly proteins, such as the Arp2/3 complex, and disassembly proteins such as cofilin and twinfilin (Hakala et al., 2021; Kanellos and Frame, 2016; Poukkula et al., 2011; Swaney and Li, 2016). By contrast, we still know very little about how this machinery controls the dynamics of actin turnover or cell behavior during collective cell movement *in vivo*.

Interestingly, despite the centrality of core actin regulators, mutation of these genes in vertebrates frequently results in surprisingly specific developmental phenotypes. For example, cofilin-null mutants display defects in morphogenesis during neural tube closure in zebrafish and mice (Grego-Bessa et al., 2015; Lin et al., 2010; Mahaffey et al., 2013), and the cofilin cofactor cyclase-associated protein (CAP, also known as CAP1 and Srv2) is required for morphogenetic cell movements during gastrulation in zebrafish (Daggett et al., 2004, 2007). Other actin regulators such as α-actinin, profilin and CARMIL are also essential for CE (Khadka et al., 2009; Shawky et al., 2018; Walck-Shannon et al., 2015). Finally, Twinfilin is required for a variety of actin-related cell behaviors in *Drosophila* (Wahlström et al., 2001; Wang et al., 2010), but its role in the dynamic control of morphogenetic cell movements in developing vertebrates has not yet been defined.

Here, using the *Xenopus* dorsal gastrula mesoderm, we explored the localization of several actin-regulatory proteins, defined the *in vivo* interactome of Cofilin2, and explored the function of the actin depolymerizing protein Twinfilin1 in CE. These data provide an important *in vivo*, developmental complement to the extensive body of biochemical and cell biological work carried out using purified twinfilins *in vitro* and provide new insights into the role of core actin regulators in cell-type-specific cell behaviors during vertebrate development.

RESULTS

We chose to study lamellipodial protrusions in the dorsal gastrula mesoderm of amphibians, the so-called dorsal marginal zone or

Journal of Cell Science (2021) 134, jcs254011. doi:10.1242/jcs.254011

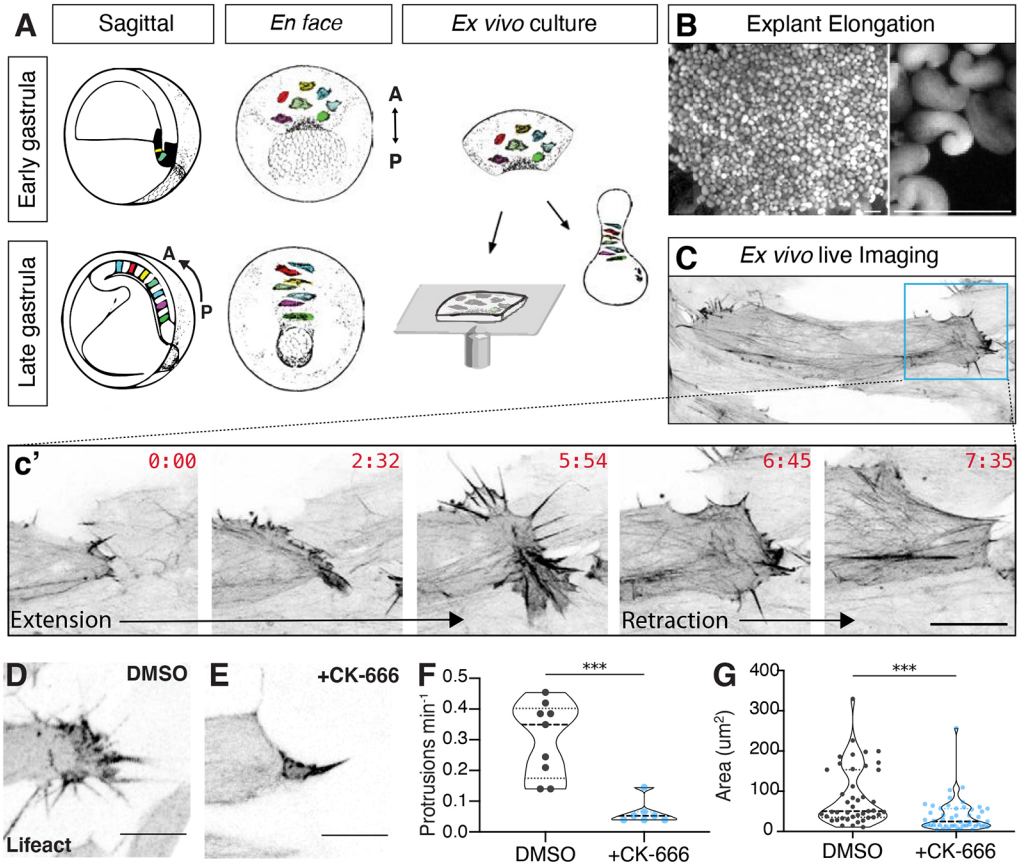

Fig. 1. Lamellipodia in the *Xenopus* DMZ. (A) Schematic showing CE cell movements and DMZ explant method. Cells are unpolarized at the start of gastrulation and over time take on a bipolar polarity and intercalate to form a longer, narrower array. (B) Image showing elongated DMZ explants, close-up is shown at right. Scale bars: 1 mm. (C) Still from time-lapse confocal microscopy showing a single round of lamellipodial extension and retraction from the mediolateral end of a single DMZ cell. (D) DMSO does not affect DMZ lamellipodia. (E) Typical effect of CK-666 on DMZ lamellipodia. (F) Quantification of effects of CK-666 on protrusion frequency. n=9 DMSO protrusions from four embryos; n=7 CK666 protrusions from three embryos. ***P<0.001 for DMSO vs CK-666 (Mann–Whitney U-test). (G) Quantification of effects of CK-666 on protrusion size. n=43 DMSO-treated protrusions from four embryos, n=49 CK-666-treated protrusions from three embryos. ***P<0.001 for DMSO vs CK-666 (Mann–Whitney U-test). Graphs in F, G are violin plots with the median being highlighted by a dashed line and quartiles with dotted lines. Scale bars: 10 µm.

DMZ (Fig. 1A), an embryonic tissue that was among the first shown to undergo autonomous CE. In the 1940s, Holtfreter and Schectman independently showed that isolated explants of this tissue robustly elongate in culture (Holtfreter, 1944; Schectman, 1942), and pioneering work from Ray Keller and colleagues using *Xenopus* provided the first cell biological insights into this elongation process (Keller and Hardin, 1987; Shih and Keller, 1992a; Wilson and Keller, 1991). Since then, the tissue has served as a central paradigm for understanding the cellular and molecular basis of CE, including several molecular studies of lamellipodial protrusive activity (e.g. Kim and Davidson, 2011; Pfister et al., 2016; Skoglund et al., 2008; Tahinci and Symes, 2003; Wallingford et al., 2000).

These protrusions differ along the deep-superficial axis of the DMZ, with large lamelliform protrusions at the surface of the tissue and smaller, confined protrusions along the junctional axis (Fig. S1). Because our interest lay in comparing lamelliform protrusions in the *Xenopus* DMZ with the far more well-characterized lamellipodia in cultured cells, we performed a series of cell biological analyses focusing exclusively on the lamelliform protrusions, best seen superficially. We manually isolated DMZ explants and cultured them *ex vivo* for explant elongation or live imaging (Fig. 1A–C), and then we used a combination of confocal and total internal reflection fluorescence (TIRF) imaging to monitor lamellipodial dynamics, protein localization and actin dynamics.

Dynamics and composition of *Xenopus* DMZ lamellipodia resemble those in single migrating cells

In cultured cells, lamellipodia are formed by branched actin networks that are assembled by the Arp2/3 complex, so we first tested the role of this complex in the *Xenopus* DMZ. We found that treatment of DMZs with the Arp2/3 inhibitor CK-666 (Nolen et al., 2009) robustly suppressed the formation of lamelliform protrusions (Fig. 1D–F), and also dramatically altered the shape of those that did form. As a simple metric, we noted that lamellipodial area was significantly reduced after CK-666 treatment (Fig. 1D,E,G).

We next sought to explore the protein interaction landscape of actin regulation specifically in the *Xenopus* DMZ. We focused this experiment on Cofilin, which has been shown to be essential for CE in both mice and fish (Gurniak et al., 2005; Lin et al., 2010; Mahaffey et al., 2013). To identify interaction partners specifically in cells normally engaged in CE, we expressed GFP-tagged Cofilin2 by mRNA injection and manually dissected ∼750 Keller explants and cultured them until Nieuwkoop and Faber (NF) stage 14 (Fig. 1A,B). Protein was isolated from these tissue explants and affinity purification mass spectrometry (APMS) was performed using an anti-GFP antibody. To control for non-specific interactions, each experiment was accompanied by a parallel APMS experiment using un-fused GFP, the results of which were then used to subtract background by calculating a Z-test and fold change for differential enrichment for each protein (Fig. 2A; see Materials and Methods).

Our APMS data revealed that Cofilin in the *Xenopus* DMZ associated with α-, β- and γ-actin (Fig. 2A; Table S1, Fig. S2), as expected and consistent with previous high-throughput protein interaction mapping in human cells (Rolland et al., 2014). Cofilin also interacted with Cyclase-Associated Protein (CAP) (Fig. 2A; Table S1), consistent with data from cultured human cells and yeast (Moriyama and Yahara, 2002; Quintero-Monzon et al., 2009). We also identified significant, but less robust, interactions with subunits of the capping protein complex (Capza and Capzb) as well as with

Journal of Cell Science (2021) 134, jcs254011. doi:10.1242/jcs.254011

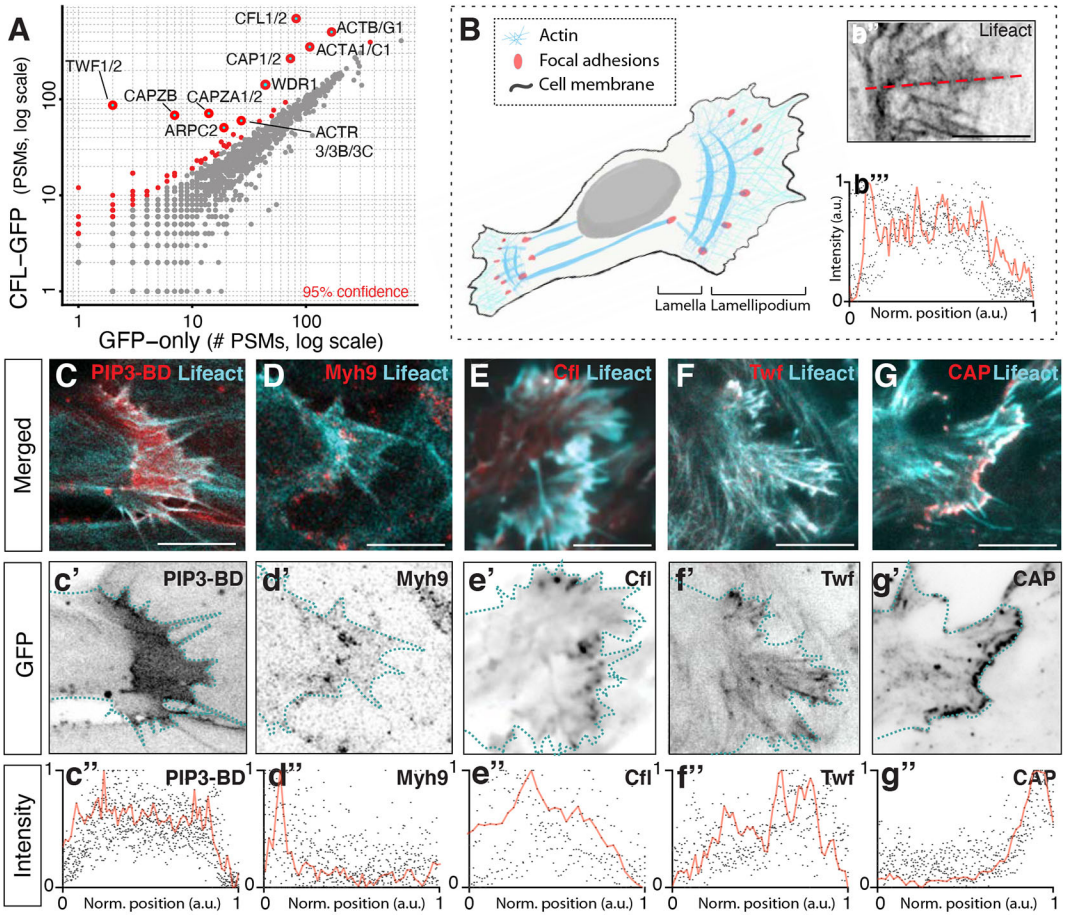

Fig. 2. Localization of lamellipodial markers. (A) Interaction partners of Cfl2 were identified based on their enrichment in APMS of the Cfl2–GFP-tagged bait protein (vertical axes) relative to APMS of the untagged GFP controls (horizontal axes). Confidence values were calculated by one-sided *Z*-test (see Materials and Methods). A pseudocount of 1 PSM was added to each protein for visualization on a log–log plot. (B) Schematic showing the quantification scheme used here. b″, red dotted line indicates line-plot measurement taken along protrusion length; b‴, trace of actin intensity along protrusion length. Red line highlights one example trace, black dots are representative of several line plots. a.u., arbitrary units. (C,c′,c″) Pip3 localization and quantification; LifeAct in the alternate channel reports actin localization. (D,d′,d″) Myh9 localization and quantification. (E,e′,e″) Localization and quantification of Cfl2; LifeAct in the alternate channel reports actin localization. (F,f′,f″) Localization and quantification of Twf1. (G,g′,g″) Localization and quantification of Cap2. Dashed lines highlight cell edges. au, arbitrary units. Images shown are representative of at least three experiments. Scale bars: 10 µm.

components of the Arp2/3 complex (Fig. 2A; Table S1). Finally, we identified significant interactions with Twinfilin1 and Twinfilin2 (Twf1 and Twf2). Of course, APMS cannot distinguish between direct and indirect interactions, and it is in fact likely that these interactions detected by APMS are mediated by association of these proteins with actin itself. Nonetheless, these results provide an *in vivo* reflection of functional interactions known to link these proteins in yeast, in mammalian cultured cells, and *in vitro* (e.g. Chaudhry et al., 2013; Goode et al., 1998; Hakala et al., 2021; Iwasa and Mullins, 2007; Johnston et al., 2015; Shekhar et al., 2019).

Next, we explored the subcellular localization of these actin-regulatory proteins. As a baseline, we quantified the localization patterns of lamellipodial markers that are well-defined *in vitro*. For example, LifeAct and a phosphatidylinositol (3,4,5)-trisphosphate (PIP3) sensor (PH domain fused to GFP; Tall et al., 2000) were both robustly enriched throughout the lamellipodia (Fig. 2B,C). By contrast, the Myosin heavy chain Myh9 was enriched specifically in the cell-proximal lamella (Fig. 2D), again similar to what has been described for single migrating cells.

We then used expression of GFP fusions to determine the localization of Cofilin and its two strongest interactors in our APMS data, Twf1 and CAP. We found that Cofilin was broadly enriched in lamellipodia of mesoderm cells in the *Xenopus* DMZ, with a slight bias for the proximal region (Fig. 2E). Twf1 was also broadly enriched but with a slightly more distal bias (Fig. 2F). In striking contrast, CAP was restricted specifically at the distal edge of the lamellipodium in these cells (Fig. 2G). These *in vivo* results are consistent with known localization of these proteins on single actin filaments *in vitro*. Specifically, Cofilin was found to bind along actin filaments but is enriched on older ADP-bound segments of actin filaments near pointed ends (Bibeau et al., 2021); Twinfilin binds filament barbed ends (Shekhar et al., 2021), and CAP is associated with barbed ends of actin filaments in the presence of Twinfilin (Johnston et al., 2015). Actin filaments within protrusions are oriented with the pointed ends at the proximal side of the protrusion and growing barbed ends at the distal side of the lamellipodia, we therefore believe the known localization of these proteins on purified actin filaments *in vitro* closely reflects our observations on the lamellipodial actin networks within protrusions *in vivo*.

Twinfilin is required for axis elongation and cell polarity establishment

We then selected Twf1 for more in-depth studies, because while loss of either CAP or cofilin in vertebrates is known to impact embryonic

Journal of Cell Science (2021) 134, jcs254011. doi:10.1242/jcs.254011

morphogenesis (Daggett et al., 2004, 2007; Gurniak et al., 2005; Lin et al., 2010; Mahaffey et al., 2013), the function of Twf1 in early vertebrate embryos has not been reported. We used morpholino (MO) oligonucleotides to disrupt splicing of the Twf1 transcript, and knockdown (KD) of Twf1 elicited a robust defect in the elongation of the embryonic axis (Fig. 3A; Fig. S3). This defect was significantly rescued by re-introduction of Twf1 mRNA (Fig. 3A; Fig. S3). As an additional control, we performed F0 knockout (KO) of Twf1 using CRISPR/Cas9, which elicited an identical phenotype (Fig. 3A; Fig. S3). Together, these orthogonal loss-of-function approaches indicate that defective axis elongation is a specific result of Twf1 loss in *Xenopus*.

Curiously, the robust elongation defect we observed in embryos lacking Twf1 was not associated with the severe dorsal flexion commonly observed following disruption of CE by manipulations of planar cell polarity (PCP) signaling (e.g. Wallingford and Harland, 2001). As a more direct test of the role of Twf1 in CE, we tested the effect of Twf1 KD on the elongation of isolated explants of the dorsal marginal zone of the *Xenopus* gastrula, which is known to be driven by CE in a tissue-autonomous manner (Keller et al., 1992). Twf1 KD elicited a dose-dependent suppression of the elongation of isolated DMZ explants (Fig. 3B; Fig. S3).

We then explored the cell biological basis of the CE defects following loss of Twf1 by examining a variety of cell behaviors. CE in the DMZ is associated with elongation of the cellular long axis, alignment of cellular long axes in the mediolateral plane and polarized positioning of lamellipodial protrusions to the mediolateral ends of cells (Shih and Keller, 1992a), and defects in these behaviors are commonly associated with defective CE (e.g. Tahinci and Symes, 2003; Wallingford et al., 2000). Simple imaging of cells labeled with Lifeact–GFP revealed that disruption of Twf1 either by MO or by CRISPR resulted in a significant reduction of cellular length-to-width ratios in the DMZ (Fig. 3C; Fig. S3) and a robust failure to properly orient the cellular long axis (Fig. 3D–G).

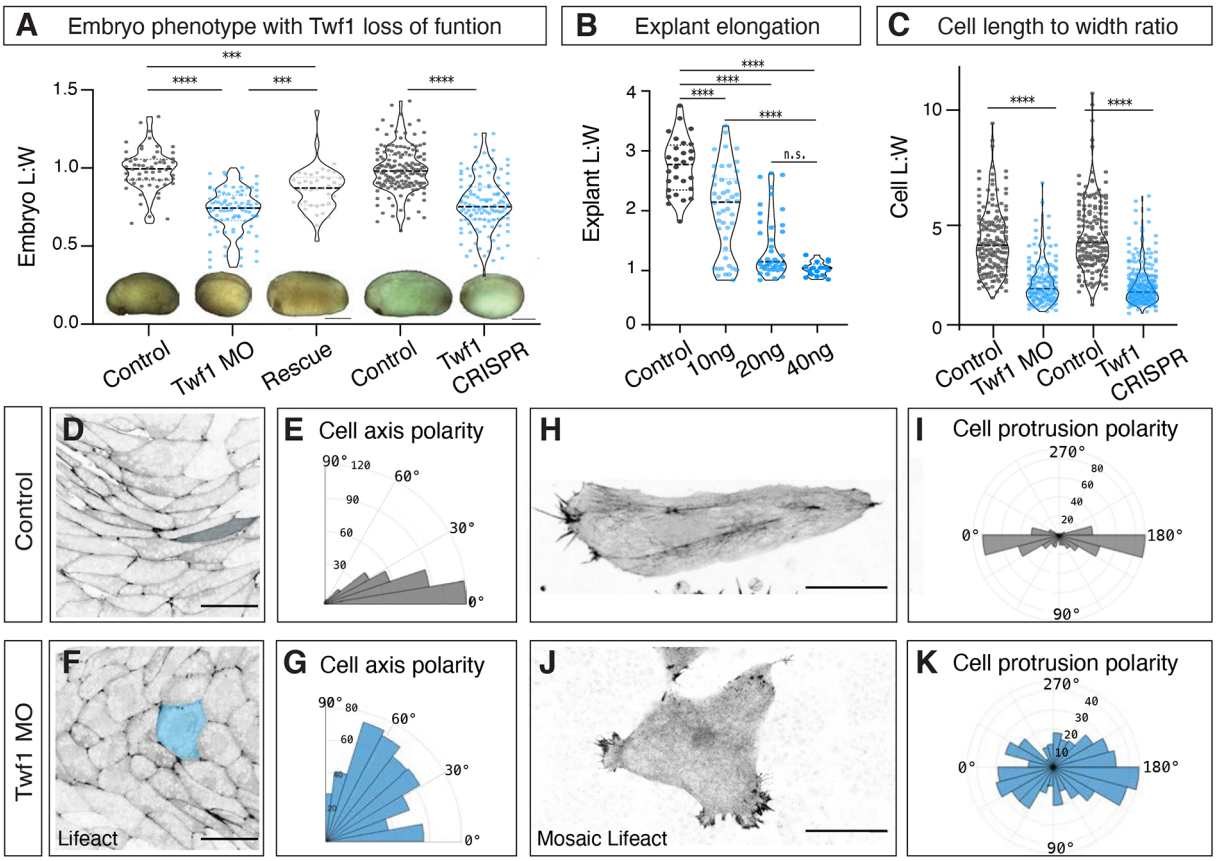

Fig. 3. Twf1 is required for axis elongation and convergent extension. (A) Quantification of axis elongation (as length/width ratio) for control, Twf1 morphants, and Twf1 mRNA rescued embryos, along with sgRNA control and Twf1 crispants (inset images show representative examples; see more embryos in Fig. S3C), *n*=60 control embryos, *n*=88 morphant embryos, *n*=43 rescue embryos, *n*=155 sgRNA control, *n*=119 Twf1 Crispr. ***P<0.001; ****P<0.0001; n.s., not significant (Kruskal–Wallis test). Scale bars: 1 mm. (B) Quantification of explant elongation (as length/width ratio) for isolated DMZs from control and Twf1 morphant embryos. *n*=28, control; *n*=46, 10 ng; *n*=41, 20 ng; *n*=17, 40 ng. ****P<0.0001 for control vs 10 ng, 20 ng, 40 ng, n.s., not significant (P=0.0966) for 20 ng versus 40 ns (one-way Kruskal–Wallis test). (C) Quantification of cell shapes for control versus Twf1 morphant, and sgRNA control and Twf1 crispant DMZs. *n*=168 control cells from six embryos, *n*=156 Twf1 morphant cells from six embryos, *n*=169 sgRNA control cells from 11 embryos, *n*=294 Twf1 Crispr cells from 14 embryos, three experiments (representative images in Fig. S3C). ****P<0.0001 (Mann–Whitney *U*-test). Graphs in A–C are violin plots with the median being highlighted by a dashed line and quartiles with dotted lines. (D,E) Representative image (D) and rose diagram (E) showing quantification of cell axis polarity in control DMZ. Scale bar: 50 µm. (F,G) Representative image (F) and rose diagram (G) showing disrupted cell axis polarity in Twf1 morphant. Scale bar: 50 µm. E,G shows control vs Twf1 morphant, *n*=387 control cells from nine embryos, *n*=522 Twf1 morphant cells from 15 embryos. P<0.0001 (Kolmogorov–Smirnov test). (H) Confocal image of mosaically labeled cell in control DMZ. Scale bar: 10 µm. (I) Rose diagram showing the normal mediolateral polarization of lamellipodia in the control DMZ. (J) Confocal image of mosaically labeled cell in Twf1 morphant DMZ. Scale bar: 10 µm. (K) Rose diagram showing the disrupted mediolateral polarization of lamellipodia in the morphant. I,K show control vs Twf1 morphant, *n*=119 control protrusions from five embryos, *n*=194 Twf1 morphant protrusions from nine embryos. P<0.0001 (Kolmogorov–Smirnov test).

Journal of Cell Science (2021) 134, jcs254011. doi:10.1242/jcs.254011

To more specifically assess the effects of Twf1 loss on lamellipodia, we used targeted microinjection to generate mosaic embryos in which cells labeled with LifeAct–GFP were surrounded by unlabeled cells, allowing unambiguous quantification of lamellipodia orientation in the DMZ (Fig. 3H,J). While lamellipodia were tightly confined to mediolateral cell faces in control DMZ explants, as expected (Shih and Keller, 1992a), this mediolateral polarity was lost when Twf1 was disrupted (Fig. 3H–K). Together, these data demonstrate that Twf1 is required for the execution of cell behaviors that drive CE in *Xenopus*.

Twinfilin is essential for the formation of specialized cortical actin structures during CE

The function of lamellipodia in driving cell movements during CE remains poorly understood as compared to its function in individual migrating cells in culture. For example, cells during CE are bipolar and consistently form lamellipodia on both ends, making the concept of a single 'leading edge' ambiguous in this context (Shih and Keller, 1992a). Moreover, lamellipodia are thought to collaborate with junction contractions to cooperatively drive the movement of cell bodies during CE in *Xenopus* (Huebner and Wallingford, 2018; Weng et al., 2021 preprint). Finally, a specialized cytoplasmic 'node-and cable' system has been described in *Xenopus* DMZ cells (Kim and Davidson, 2011; Pfister et al., 2016; Skoglund et al., 2008). How this system relates to the actin cortex of single migrating cells (i.e. stress fibers, etc.) remains unknown, and how the dynamics of the DMZ node and cable system may integrate lamellipodial activity and junction contraction (e.g. Shindo et al., 2019) is unclear.

We therefore used TIRF imaging to ask how Twf1 loss impacts the node and cable system in the DMZ. In normal cells, these actin cables are strongly aligned in the mediolateral axis of the cell (Kim and Davidson, 2011; Skoglund et al., 2008). Using the Orientation J plugin in Fiji (Püspöki et al., 2016), we observed robust mediolateral polarity of actin cables, as expected (Fig. 4A,a′,C). By contrast, this polarization was significantly disrupted by Twf1 loss, with cables displaying a near random orientation (Fig. 4B,b′,C). Interestingly, we did not observe Twf1 enrichment to the actin cables themselves (not shown), consistent with the absence of Twf1 at mammalian stress fibers (Vartiainen et al., 2000). These results suggest that the defects in actin cable polarity are likely secondary to the defects in lamellipodial position or dynamics.

Twinfilin controls lamellipodial size and dynamics

To better understand how Twf1 function in lamellipodia may impact cell polarization during CE, we next sought to quantify the effects of Twf1 loss on the dynamic behavior of lamellipodia. This is an important unanswered question, because while it has been extensively studied in biochemical terms, we still know little about the role of twinfilins in living tissues. For example, loss of Twinfilin in *Drosophila* S2 cells in culture results in enlarged lamellipodia with altered actin dynamics, and similar results were recently reported in B16-F1 mouse melanoma cells (Hakala et al., 2021; Iwasa and Mullins, 2007). There are as of yet no reports of the impact of Twf1 loss on lamellipodial dynamics in an intact tissue *in vivo*.

In the *Xenopus* DMZ, we found that Twf1 loss did not impact the overt morphology of lamellipodia (Fig. 5A,B), but did severely disrupt the dynamics of lamellipodial assembly – Twf1 KD cells initiated lamellipodial extension less frequently (Fig. 5C). Moreover, although extension rates were not altered (Fig. 5D), lamellipodia spent relatively more time elongating compared to controls (Fig. 5E). Lamellipodia retraction times were not different between control and Twf1 KD (Fig. 5E), and, accordingly, the mean size of lamellipodia in these cells was significantly larger (Fig. 5F).

Twinfilin is required for rapid actin turnover and dynamic actin treadmilling

Finally, we sought to link the extensive previous biochemical characterization of twinfilin to the *in vivo* functions we describe here. In *in vitro* assays using single actin filaments, the mechanisms by which Twf and its associated factors tune depolymerization have been extensively characterized (e.g. Hakala et al., 2021; Hilton et al., 2018; Johnston et al., 2015; Shekhar et al., 2021). However, the rates of actin turnover vary considerably between *in vitro* studies and those in living cells (Miyoshi and Watanabe, 2013), so we sought to quantify actin turnover *in vivo* specifically during *Xenopus* CE and to assess the impact of Twf1 loss.

To this end, we developed methods to perform actin fluorescent speckle microscopy *in vivo* using DMZ explants (Fig. 6A). We injected fluorescently labeled actin monomers (Alexa Fluor 568-conjugated actin) into four-cell stage *Xenopus* embryos, and imaged DMZ explants using TIRF microscopy. We titrated the dose of injected actin until we achieved appropriate mosaic distribution of speckles, which in our hands was 0.1 ng injected per blastomere. By measuring the lifetime of individual actin speckles as they were incorporated and removed from the treadmilling actin network, we found that actin speckle lifetimes were significantly increased by Twf1 disruption in *Xenopus* gastrula mesoderm (Fig. 6B–D), consistent with actin speckle data from *Drosophila* S2 cells in culture (Iwasa and Mullins, 2007). Our result is also consistent with

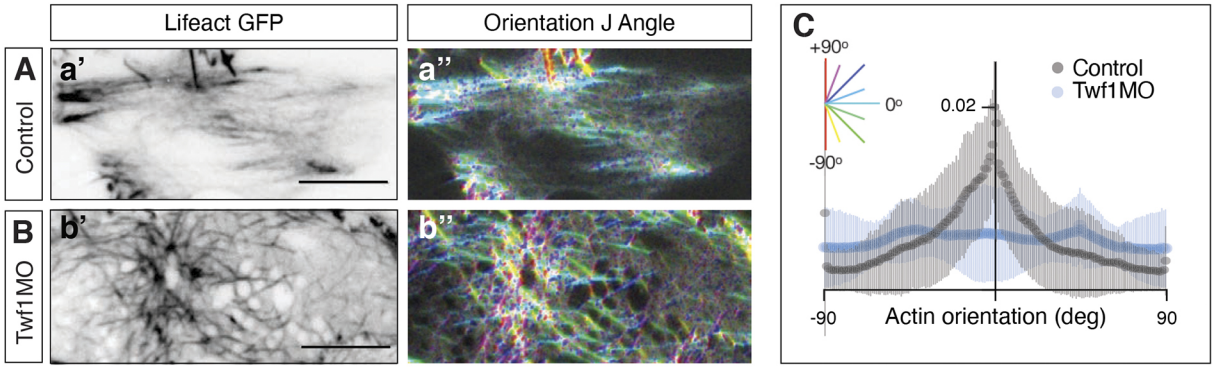

Fig. 4. Twinfilin is required for actin node and cable formation. (A,B) TIRF images of actin cables in control and Twf1 morphant DMZ cells. In right-hand panels, color reflects orientation of cables as indicated by the legend in C. (C) Quantification of actin cable organization in control and Twf1 morphants. *n*=6 control embryos, *n*=11 Twf1 morphant embryos. *P*<0.0001 for control vs Twf1 morphant (Kolmogorov–Smirnov test). Scale bars: 10 µm.

Journal of Cell Science (2021) 134, jcs254011. doi:10.1242/jcs.254011

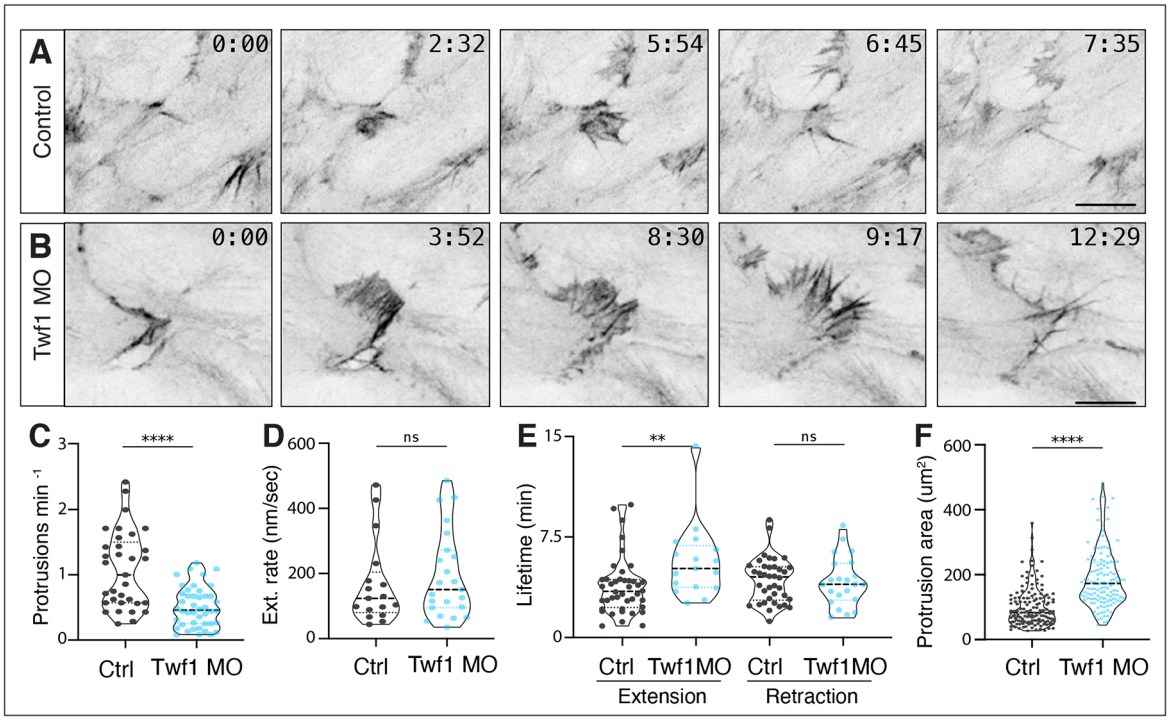

Fig. 5. Twf1 controls lamellipodial dynamics in the *Xenopus* DMZ. (A,B) Confocal images of single cells in a LifeAct–GFP-expressing control and Twf1 morphant DMZ. Scale bars: 10 µm. (C) Quantification of lamellipodial protrusion frequency for control and Twf1 morphants. Control versus Twf1 morphant, *n*=33 control protrusions from two embryos; DMSO, *n*=44 Twf1 morphant protrusions from four embryos. ****P<0.0001 (Mann–Whitney *U*-test). (D) Quantification of lamellipodial extension rate. *n*=17 control protrusions from four embryos; *n*=23 Twf1 morphant protrusions from five embryos. n.s., not significant for control vs Twf1 morphant (P=0.516; Mann–Whitney *U*-test). (E) Quantification of lamellipodial extension and retraction lifetimes. *n*=42 control protrusions from four embryos; *n*=22 Twf1 morphant protrusions from six embryos. **P<0.01 for control vs Twf1 morphant, extension lifetime; n.s., not significant, for control vs Twf1 morphant retraction lifetime (Mann–Whitney *U*-test). (F) Quantification of lamellipodial area for control and Twf1 morphants. *n*=144 control protrusions from three embryos, *n*=127 Twf1 morphant protrusions from six embryos. ****P<0.0001 for control vs Twf1 morphant (Mann–Whitney *U*-test). Graphs in C–F are violin plots with the median being highlighted by a dashed line and quartile with dotted lines.

recent fluorescence recovery after photobleaching (FRAP) data on actin turnover in mouse melanoma cells (Hakala et al., 2021).

Our data are also consistent with *in vitro* data showing that Twf specifically accelerates depolymerization at barbed ends of newly polymerized actin filaments under conditions similar to the protrusion extension phase (i.e. in the presence of polymerizable actin monomers) (Shekhar et al., 2021). Twf has been suggested to transiently bind barbed ends and depolymerize actin filaments, leaving barbed ends to oscillate between a growing state (when no Twf is bound) and a depolymerizing state (when Twf is bound) (Johnston et al., 2015; Shekhar et al., 2021). In the context of protrusions during CE, we believe the presence of Twf tempers protrusion extension by reducing effective barbed end elongation. In the absence of Twinfilin, barbed ends would continue to polymerize unhindered, leading to more stable filaments (Fig. 6D) and longer protrusion extension times (Fig. 5E).

Finally, we asked how the observed changes in actin dynamics after Twf1 loss might relate to the localization of other actin regulators. Based on the distal localization of Twf1 and CAP1 as well as *in vitro* data suggesting a preference for simultaneous binding of Twf and CAP to filament barbed ends (Johnston et al., 2015), we asked how CAP1 localization is affected by the absence of Twf1. In control cells, as mentioned above, CAP1 is strongly enriched at the distal edge of lamellipodia (Fig. 2G; Fig. 6E,F). By contrast, this distal restriction was lost after Twf1 knockdown, and we instead observed CAP1 localization throughout the lamellipodium (Fig. 6G,H). The change in distribution of CAP1 after Twf1 KD was highly significant as compared to controls. This result is consistent with an earlier *in vitro* study which showed an increase in Twinfilin's barbed end residence times was associated with presence of CAP, thus indicating that Twinfilin might help localize CAP to actin filament barbed ends (Johnston et al., 2015). Together with those previous reports, our findings argue that the cellular functions of Twf1 in both lamellipodial dynamics and actin turnover are evolutionarily conserved in *Xenopus*, *Drosophila* (Iwasa and Mullins, 2007), and mice (Hakala et al., 2021). Further *in vivo* characterization of Twf1, as well as related factors such as CAP and cofilin therefore should be illuminating.

DISCUSSION

Several previous studies have demonstrated surprisingly specific morphogenetic phenotypes associated with loss of fundamental actin regulators. Here, we show that many elements of lamellipodia-related protein localization and protein-protein interactions defined in single cells in culture are conserved in cells of the *Xenopus* DMZ during CE, and more importantly, we provide the first analysis of twinfilin function in dynamic cell behaviors in a vertebrate *in vivo*. We show not only that loss of Twf1 results in defects in the dynamics of actin turnover and lamellipodial shape, but also in defects in the polarized alignment of specialized cortical actin cables in these cells.

Interestingly, while our *in vivo* results confirm several results obtained previously in cell culture, we believe the findings are important because both the regulation (i.e. by PCP proteins) and the

Journal of Cell Science (2021) 134, jcs254011. doi:10.1242/jcs.254011

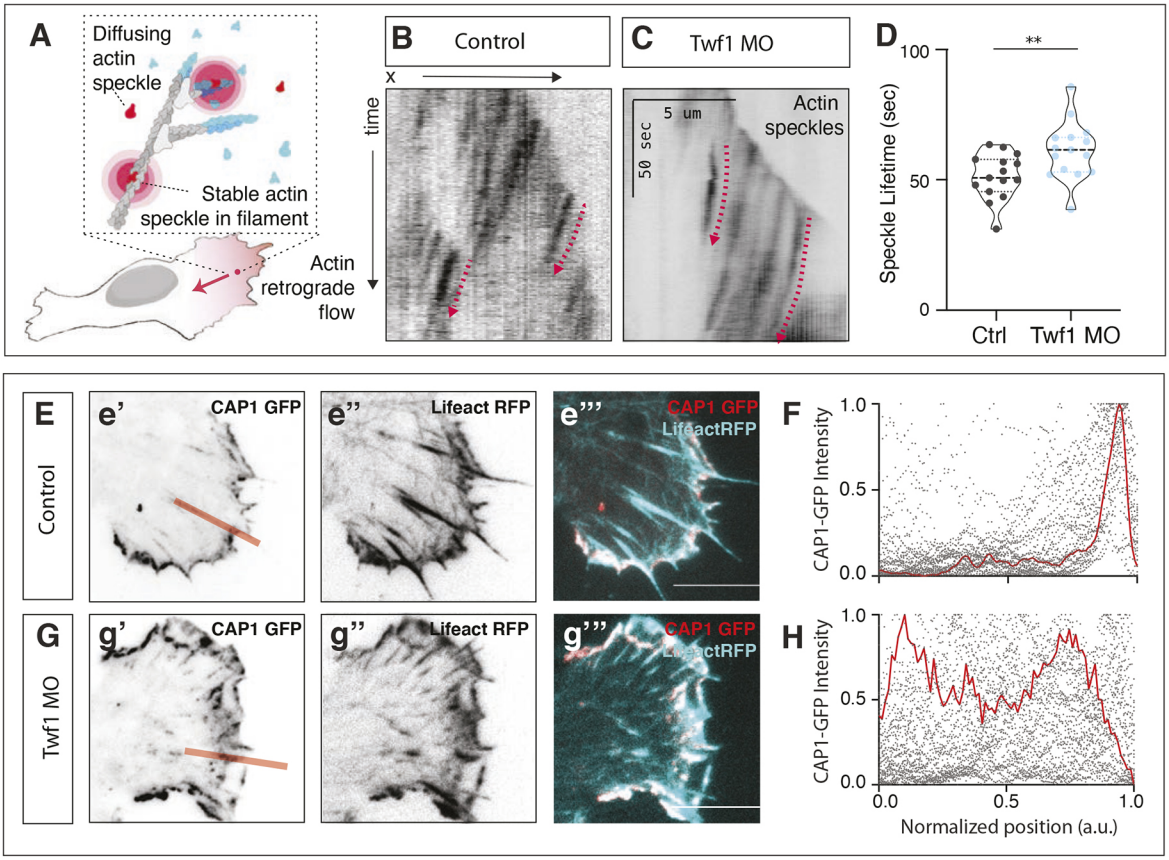

Fig. 6. Twinfilin regulates actin turnover in protrusions during CE. (A) Schematic of fluorescent speckle imaging. (B,C) Kymograph from TIRF movies showing fluorescent actin speckles in lamellipodia in control and Twf1 morphant *Xenopus* DMZs. Scale (*x*, distance): 5 µm, scale (*y*, time): 50 s. (D) Quantification of actin speckle lifetimes. *n*=15 control protrusions from three embryos; *n*=15 Twf1 morphant protrusions from six embryos. ***P*<0.01 for control vs Twf1 morphant (Mann–Whitney *U*-test). Graph is violin plots with the median being highlighted by a dashed line and quartiles with dotted lines. (E) Cap localization in control protrusion; LifeAct in the alternate channel reports actin localization. Red line indicates line-plot measurement taken along protrusion length. (F) Quantification of distally restricted Cap localization in control protrusion. Red line highlighting one example trace, black dots representative of several line plots. (G) Cap localization in Twf1 morphant protrusion. (H) Quantification showing expansion of distal bias of Cap localization in Twf1 morphant cells. Scale bars: 10 µm, unless otherwise noted. (G,H) Cap1 distribution in Control vs Twf1 morphant was significantly different. *n*=36 protrusions from eight control embryos; *n*=28 cells from nine Twf1 morphant embryos. *****P*<0.0001 (Kolmogorov–Smirnov test). a.u., arbitrary units.

function of lamellipodia during CE are highly specialized (Huebner and Wallingford, 2018). For example, we find that DMZ cells lacking Twf1 function fail to elongate mediolaterally (Fig. 3), a phenotype also observed with disruption of either PCP or Rho signaling, but not Rac signaling (Tahinci and Symes, 2003; Wallingford et al., 2000), potentially suggesting links between the former proteins and Twf1.

Directly connecting the observed actin phenotype after Twf1 loss to the aggregate embryo phenotype is more difficult, but could be explained in several different ways. While we only observed enrichment of Twf1 in protrusions, Twf1 may play an essential role in actin turnover in the cortical actin network that directly impacts cellular actin cable alignment. In this case, Twf1 may be required to connect the actin network in protrusions with that of the cortical actin network, a process that has been described in single migrating cells and the context of CE, but remains poorly defined (e.g. Hotulainen and Lappalainen, 2006; Kim and Davidson, 2011; Shindo et al., 2019). This hypothesis is particularly intriguing as others have shown an accumulation of actin at the base of protrusions in Twf KO cells (Hakala et al., 2021).

Additionally, a coordinated cycle of actomyosin contractions in protrusions and cortical actin has been demonstrated in converging and extending cells (Kim and Davidson, 2011; Shindo et al., 2019). Because we have previously shown that altering the timing of these contractions is sufficient to disrupt CE (Shindo et al., 2019), changes in the duration of protrusions after Twf1 loss might also alter this dynamic interplay of actin populations. Moreover, how force for cell body displacement is achieved during CE remains a contentious issue (Huebner and Wallingford, 2018), so our finding that specific disruption of lamellipodial dynamics following Twf1 disruption is associated with failure to polarize cytoplasmic actin cables in the DMZ is also significant. Asking how Twf1 loss impacts junction contraction in these cells will be an interesting next step. Overall, studying Twf1 in this tissue and parsing these ideas will greatly extend our knowledge of Twf1 function.

These data also add to a growing body of work linking specific actin regulatory machinery to essential cell behaviors during development. As discussed, actin severing and depolymerizing proteins cofilin (Mahaffey et al., 2013; Grego-Bessa et al., 2015), CAP (Daggett et al., 2004), and now twinfilin have been identified to play a role in CE. Additionally, the upstream actin regulators Rac and Rho control polarized protrusive activity in *C. elegans* and vertebrate models (Tahinci and Symes, 2003; Walck-Shannon et al., 2015). The actin sequestering profilins are also essential for gastrulation, although interestingly, profilin 1 and 2 are required for gastrulation, but only profilin 2 is required for CE movements (Khadka et al.,

2009). Finally, the actin crosslinking protein α-actinin is involved in regulating cell polarity during gastrulation (Shawky et al., 2018). This mounting evidence strongly suggests that specialized functions of actin regulatory machinery are carefully deployed during CE and highlight the need for cell type-specific studies of actin-related proteins during specific cell movements *in vivo*.

Ultimately, these data advance our goal of developing an integrated view of the molecular mechanisms linking the ubiquitous and evolutionarily conserved machinery of actin regulation to the highly specialized behaviors of diverse cell types in vertebrate animals.

MATERIALS AND METHODS

Xenopus embryo manipulations

Xenopus laevis females were super-ovulated by injection of 500 units of human chorionic gonadotropin (hCG) (Chorulon hCG, Cat no. 16951247, Merck Animal Health, Madison, NJ, USA). The following day, eggs were squeezed from the females. *In vitro* fertilization was performed by homogenizing a small part of a harvested testis in 1× Marc's modified Ringer's (MMR) and mixing with collected eggs. Embryos were dejellied in 3% cysteine (pH 7.9) at the two-cell stage. Fertilized embryos were rinsed and reared in 1/3× MMR solution. For microinjections, embryos were placed in a 2% ficoll in 1/3× MMR solution and injected using forceps and an Oxford universal micromanipulator. MO oligonucleotide or CRISPR/Cas9 was injected into two dorsal blastomeres to target the dorsal marginal zone (DMZ). Embryos were microinjected with mRNA at the four-cell stage for uniform labeling and at the 32- to 64-cell stage for mosaic labeling. Embryos were staged according to Nieuwkoop and Faber (1994). All animal work has been approved by the IACUC of UT, Austin, protocol no. AUP-2012-00156.

Plasmids, mRNA, protein and MOs for microinjections

Xenopus gene sequences were obtained from Xenbase (www.xenbase.org) and open reading frames (ORF) of genes were amplified from the *Xenopus* cDNA library by PCR, and then are inserted into a pCS10R vector fused with C-terminal GFP. CS10R is an in-house, artisanal vector derived from the CS2 family of plasmids for gene expression in *Xenopus* (http://cshprotocols.cshlp.org/content/2010/5/pdb.prot5427.full). This vector is available from the authors upon request. The following constructs were cloned into the pCS vector: Twf1–GFP, CAP1–GFP and Cfl2–GFP. These constructs were linearized and the capped mRNAs were synthesized using mMESSAGE mMACHINE SP6 transcription kit (ThermoFisher Scientific, Waltham, MA, USA). Concentration for GFP localization was titrated to lowest concentration where we could still detect GFP signal, but no cellular phenotype was observed. The amount of injected mRNAs per blastomere are as follows: Lifeact–GFP or –RFP (50–100 pg), PIP3–PBD (25 pg; Tall et al., 2000), Myl9–GFP (20 pg; Shindo and Wallingford, 2014), Twf1–GFP (25 pg for imaging, 1 ng for rescue), Cap1–GFP (25 pg) and Cfl2 (25 pg).

Twf1 morpholino was designed to target exon-intron splicing junction (Gene Tools, Philomath, OR, USA). The MO sequences and the working concentrations was 5′-TGAGTCAAAACACTTACATGGGAGT-3′ and 10 ng per injection unless otherwise noted.

CRISPR sgRNAs were designed to target exon 2 using the online design tool CHOPCHOP (Labun et al., 2019). Synthetic sgRNA was ordered from Synthego (Menlo Park, CA, USA) and combined with Cas9 protein (PNABIO, Cat no CP01, Newbury Park, CA, USA) prior to injection at four-cell stage. Two individual targets were tested in isolation (250 pg/10 nl injection) and pooled (125 pg each), each giving the same embryonic phenotype. Pooled sgRNAs were used for all experiments. The sgRNA sequences and working concentrations were: Twf1 Target 1, 5′-ACC-AAAUUCCUUCUUCACAGUGG-3′ (125 pg/10 nl injection); Twf1 Target 2, 5′-AAAAUGCGCAAGGCUUCGAGUGG-3′ (125 pg/10 nl injection); Cas9 protein (1 ng/10 nl injection).

For fluorescent actin speckle microscopy, labeled actin monomers (Alexa Fluor 568-conjugated actin, catalog number A12374, Thermo Fisher Scientific, Waltham, MA, USA) were reconstituted in a 2 mg/ml stock solution. A 0.01 µg/µl working solution was prepared for each 10 nl injection, and 0.1 ng was injected into dorsal blastomeres of four-cell stage embryos. This concentration was determined empirically by titrating the amount injected until no cellular phenotype was observed and labeled actin monomers were sparse enough to detect individual 'speckles' (Watanabe and Mitchison, 2002).

RT-PCR

To verify the efficiency of Twf1 MOs, MOs were injected into all cells at the four-cell stage and total RNA was isolated using the TRIZOL reagent (Invitrogen, Carlsbad, CA, USA) at stage 14. cDNA was synthesized using M-MLV Reverse Transcriptase (Invitrogen, Carlsbad, CA, USA) and random hexamers. Twf1 cDNAs were amplified by Taq polymerase (NEB, Ipswich, MA, USA) with the following primers: Twf1F, 5′-ACACCAGA-CACTTCAAGGAATAG-3′ and Twf1R, 5′-GGTTCTTGCAGCTGGAG-TATAA-3′; ODC 426F, 5′-GGCAAGGAATCACCCGAATG-3′ and ODC 843R, 5′-GGCAACATAGTATCTCCCAGGCTC-3′.

Embryo phenotyping and Keller explant elongation assay

To determine the morpholino oligonucleotide concentration to use, we used a dose curve and chose the lowest concentration of morpholino while maintaining consistent phenotype, deciphered based on embryo and explant phenotypes (Fig. S3). Embryo and Keller explant length and width measurements were taken in Fiji, as previously described (Shih and Keller, 1992b; Wallingford et al., 2000).

Live imaging of Keller explants

mRNAs were injected at the dorsal side of four-cell stage embryos, and the DMZ tissues were dissected out at stage 10.5 using forceps, hairloops, and eyebrow hair knives. Each explant was mounted to a fibronectin-coated dish in Steinberg's solution (Shindo and Wallingford, 2014), and cultured at 16°C for half a day before imaging with a Zeiss LSM700 confocal microscope (Jena, Germany), or Nikon N-STORM combined TIRF/STORM microscope (Minato City, Tokyo, Japan). Arp2/3-mediated actin polymerization was inhibited by incubating for 10 min with 50 µM CK-666 (Sigma, cat no. SML0006, CAS Number: 442633-00-3, St. Louis, MO, USA).

Image analysis

Images were processed with the Fiji distribution of ImageJ and Photoshop (Adobe) software suites, and figures were assembled in Illustrator (Adobe). Cell length and width measurements and protrusion angles were manually taken in Fiji along the long axis and through the centroid of the cell. To define the area of individual protrusions, custom scripts (available upon request) were written in Matlab to create a binary mask with uniform threshold, define individual protrusions and count the number of pixels representing the area of individual protrusions. Actin cable orientations were taken from TIRF images using the OrientationJ plugin in Fiji (Püspöki et al., 2016) (http://bigwww.epfl.ch/demo/orientation/). Fluorescent actin speckle lifetime measurements were taken by tracking individual speckles using MosaicSuite (http://mosaic.mpi-cbg.de) object tracking plugin in Fiji. Custom scripts were written in Matlab to count the lifetime of each speckle. Statistical analyses were carried out using Prism (Graphpad, San Diego, CA, USA) software. Each experiment was conducted on multiple days and included biological replicates. Due to non-normality observed and low *n*-number in some observations, we used non-parametric tests for statistical comparisons throughout the article. We used Mann–Whitney *U*-tests, Kruskal–Wallis tests, or Kolmogorov–Smirnov tests for statistical comparisons of two groups, multiple groups or distributions, respectively.

Immunoprecipitation from *Xenopus* DMZs for mass spectrometry

mRNA encoding GFP-only or Cfl2–GFP was injected into two dorsal blastomeres of the four-cell stage *Xenopus* embryo. Approximately 1000 DMZs per sample were isolated from stage 10.5 embryos using forceps and microblades and were cultured in 1× Steinberg's solution (0.58 mM NaCl, 0.64 mM KCl, 0.33 mM $Ca(NO_2)_2$, 0.8 mM $MgSO_4$, 5 mM Tris-HCl pH 7.4–7.6, 50 µg/ml gentamicin) until stage-matched embryos reached stage

14. The cultured explants were collected and immunoprecipitation (IP) was performed using GFP-Trap Agarose Kit (ChromoTek, cat# gtak-20, Munich, Germany). Immunoprecipitated proteins were eluted in 2× sample buffer.

Affinity purification-mass spectrometry

Immunoprecipitated proteins were resuspended in SDS-PAGE sample buffer and heated 5 min at 95°C before loading onto a 7.5% acrylamide mini-Protean TGX gel (BioRad, Hercules, CA, USA). After 7 min of electrophoresis at 100 V, the gel was stained with Imperial Protein stain (Thermo, Waltham, MA, USA) according to manufacturer's instructions. The protein band was excised, diced to 1 mm cubes and processed by standard trypsin in-gel digest methods for mass spectrometry. Digested peptides were desalted with Hypersep Spin Tip C-18 columns (Thermo Scientific, Waltham, MA, USA), dried, and resuspended in 60 µl of 5% acetonitrile, 0.1% acetic acid for mass spectrometry.

Mass spectrometry was performed on a Thermo Orbitrap Fusion Lumos Tribrid mass spectrometer (Waltham, MA, USA), using a data-dependent acquisition strategy and four technical replicates per sample. Peptides were separated using a 60-min gradient reverse phase chromatography method on a Dionex Ultimate 3000 RSLCnano UHPLC system (Thermo Fisher Scientific) with a C18 trap to Acclaim C18 PepMap RSLC column (Dionex; Thermo Fisher Scientific). Scans were acquired in rapid scan mode using a top-speed method with dynamic exclusion after 1 time for 20 s and stepped HCD collision energies of 27, 30 and 33%.

Raw MS/MS spectra were processed using Proteome Discoverer (v2.3) (Thermo Scientific, Waltham, MA, USA). We used the Percolator node in Proteome Discoverer to assign unique peptide spectral matches (PSMs) at false discovery rate (FDR)<5% to the composite form of the *X. laevis* reference proteome described in Drew et al. (2020). In order to identify proteins statistically significantly associated with Cfl2, we calculated both a log2 fold-change and a Z-score for each protein based on the observed PSMs in the Cfl2–GFP experimental pulldown relative to the GFP-only control pulldown. We calculated significance for protein enrichment in the experiment relative to control using a one-sided *Z*-test as in Lu et al. (2007) with a 95% confidence threshold ($z \geq 1.645$). We observed high concordance between technical replicates (Fig. S1).

Acknowledgements

We would like to acknowledge the Microscopy and Imaging Facility of the Center for Biomedical Research Support at The University of Texas at Austin for use of equipment and specifically thank Anna Webb and Julie Hayes for assistance and technical expertise. We thank Anna Battenhouse for advice on proteomic analyses and Daniel Dickinson for use of his TIRF microscope. We thank National *Xenopus* Resource (RRID:SCR_013731) for knowledge gained from the *Xenopus* genome editing course. And a big thank you to all of the members of the Wallingford lab for their advice and critical feedback, and especially Shinuo Weng for editing assistance!

Competing interests

The authors declare no competing or financial interests.

Author contributions

Conceptualization: C.C.D., J.B.W.; Methodology: C.C.D., C.L., O.P., R.M.C.; Software: R.M.C., E.M.M., J.A., C.C.D.; Formal analysis: C.C.D., J.A., R.M.C., E.M.M.; Investigation: C.C.D., C.L., O.P.; Data curation: C.C.D., R.M.C.; Writing - original draft: J.B.W., C.C.D.; Writing - review & editing: J.B.W., C.C.D., S.S.; Visualization: C.C.D.; Supervision: E.M.M., J.B.W.; Project administration: E.M.M., J.B.W.; Funding acquisition: E.M.M., J.B.W.

Funding

This work was supported by the Eunice Kennedy Shriver National Institute of Child Health and Human Development (NICHD) (R01HD099191, 1R21HD103882) and the National Institute of General Medical Sciences (NIGMS) (R01GM104853). E.M.M. also acknowledges support from the National Institutes of Health (R35GM122480) and Welch Foundation (F-1515). Deposited in PMC for release after 12 months.

Data availability

Proteomics data have been deposited into the MassIVE repository (accession MSV000086057) and ProteomeXchange (accession PXD021258).

Peer review history

The peer review history is available online at https://journals.biologists.com/jcs/article-lookup/doi/10.1242/jcs.254011

References

Bibeau, J. P., Gray, S. and De La Cruz, S. (2021). Clusters of a few bound cofilins sever actin filaments. *J. Mol. Biol.* **433**, 166833. doi:10.1016/j.jmb.2021.166833

Carlier, M. F., Pernier, J., Montaville, P., Shekhar, S. and Kühn, S. (2015). Control of polarized assembly of actin filaments in cell motility. *Cell. Mol. Life Sci.* **72**, 3051-3067. doi:10.1007/s00018-015-1914-2

Chaudhry, F., Breitsprecher, D., Little, K., Sharov, G., Sokolova, O. and Goode, B. L. (2013). Srv2/cyclase-associated protein forms hexameric shurikens that directly catalyze actin filament severing by cofilin. *Mol. Biol. Cell.* **24**, 31-41. doi:10.1091/mbc.e12-08-0589

Daggett, D. F., Boyd, C. A., Gautier, P., Bryson-Richardson, R. J., Thisse, C., Thisse, B., Amacher, S. L. and Currie, P. D. (2004). Developmentally restricted actin-regulatory molecules control morphogenetic cell movements in the zebrafish gastrula. *Curr. Biol.* **14**, 1632-1638. doi:10.1016/j.cub.2004.08.024

Daggett, D. F., Domingo, C. R., Currie, P. D. and Amacher, S. L. (2007). Control of morphogenetic cell movements in the early zebrafish myotome. *Dev. Biol.* **309**, 169-179. doi:10.1016/j.ydbio.2007.06.008

Devreotes, P. N., Bhattacharya, S., Edwards, M., Iglesias, P. A., Lampert, T. and Miao, Y. (2017). Excitable signal transduction networks in directed cell migration. *Annu. Rev. Cell Dev. Biol.* **33**, 103-125. doi:10.1146/annurev-cellbio-100616-060739

Drew, K., Lee, C., Dang, V., Papoulas, O., Cox, R. M., Huizar, R. L., Marcotte, E. M. and Wallingford, J. B. (2020). A systematic, label-free method for identifying RNA-associated proteins in vivo provides insights into vertebrate ciliary beating machinery. *Dev. Biol.* **467**, 108-117. doi:10.1016/j.ydbio.2020.08.008 (In Press).

Gardel, M. L., Schneider, I. C., Aratyn-Schaus, Y. and Waterman, C. M. (2010). Mechanical integration of actin and adhesion dynamics in cell migration. *Annu. Rev. Cell Dev. Biol.* **26**, 315-333. doi:10.1146/annurev.cellbio.011209.122036

Goode, B. L., Drubin, D. G. and Lappalainen, P. (1998). Regulation of the cortical actin cytoskeleton in budding yeast by twinfilin, a ubiquitous actin monomer-sequestering protein. *J. Cell Biol.* **142**, 723-733. doi:10.1083/jcb.142.3.723

Grego-Bessa, J., Hildebrand, J. and Anderson, K. V. (2015). Morphogenesis of the mouse neural plate depends on distinct roles of cofilin 1 in apical and basal epithelial domains. *Development* **142**, 1305-1314.

Gurniak, C. B., Perlas, E. and Witke, W. (2005). The actin depolymerizing factor n-cofilin is essential for neural tube morphogenesis and neural crest cell migration. *Dev. Biol.* **278**, 231-241. doi:10.1016/j.ydbio.2004.11.010

Hakala, M., Wioland, H., Tolonen, M., Kotila, T., Jegou, A., Romet-Lemonne, G. and Lappalainen, P. (2021). Twinfilin uncaps filament barbed ends to promote turnover of lamellipodial actin networks. *Nat. Cell Biol.* **23**, 147-159. doi:10.1038/s41556-020-00629-y

Hilton, D. M., Aguilar, R. M., Johnston, A. B. and Goode, B. L. (2018). Species-specific functions of Twinfilin in actin filament depolymerization. *J. Mol. Biol.* **430**, 3323-3336. doi:10.1016/j.jmb.2018.06.025

Holtfreter, J. (1944). A study of the mechanics of gastrulation, Part II. *J. Exp. Zool* **95**, 171-212. doi:10.1002/jez.1400950203

Hotulainen, P. and Lappalainen, P. (2006). Stress fibers are generated by two distinct actin assembly mechanisms in motile cells. *J. Cell Biol.* **173**, 383-394. doi:10.1083/jcb.200511093

Huebner, R. J. and Wallingford, J. B. (2018). Coming to consensus: a unifying model emerges for convergent extension. *Dev. Cell* **46**, 389-396. doi:10.1016/j.devcel.2018.08.003

Iwasa, J. H. and Mullins, R. D. (2007). Spatial and temporal relationships between actin-filament nucleation, capping, and disassembly. *Curr. Biol.* **17**, 395-406. doi:10.1016/j.cub.2007.02.012

Johnston, A. B., Collins, A. and Goode, B. L. (2015). High-speed depolymerization at actin filament ends jointly catalysed by Twinfilin and Srv2/CAP. *Nat. Cell Biol.* **17**, 1504. doi:10.1038/ncb3252

Kanellos, G. and Frame, M. C. (2016). Cellular functions of the ADF/cofilin family at a glance. *J. Cell Sci.* **129**, 3211-3218. doi:10.1242/jcs.187849

Keller, R. and Hardin, J. (1987). Cell behaviour during active cell rearrangement: evidence and speculations. *J. Cell Sci. Suppl.* **8**, 369-393. doi:10.1242/jcs.1987.Supplement_8.21

Keller, R., Shih, J. and Domingo, C. (1992). The patterning and functioning of protrusive activity during convergence and extension of the Xenopus organiser. *Development* **116**, 81-91. doi:10.1242/dev.116.Supplement.81

Khadka, D. K., Liu, W. and Habas, R. (2009). Non-redundant roles for Profilin2 and Profilin1 during vertebrate gastrulation. *Dev. Biol.* **332**, 396-406. doi:10.1016/j.ydbio.2009.06.008

Kim, H. Y. and Davidson, L. A. (2011). Punctuated actin contractions during convergent extension and their permissive regulation by the non-canonical Wnt-signaling pathway. *J. Cell Sci.* **124**, 635-646. doi:10.1242/jcs.067579

Labun, K., Montague, T. G., Krause, M., Torres Cleuren, Y. N., Tjeldnes, H. and Valen, E. (2019). CHOPCHOP v3: expanding the CRISPR web toolbox beyond genome editing. *Nucleic Acids Res.* **47**, W171-W174. doi:10.1093/nar/gkz365
Lawson, C. D. and Ridley, A. J. (2018). Rho GTPase signaling complexes in cell migration and invasion. *J. Cell Biol.* **217**, 447-457. doi:10.1083/jcb.201612069
Lin, C. W., Yen, S. T., Chang, H. T., Chen, S. J., Lai, S. L., Liu, Y. C., Chan, T. H., Liao, W. L. and Lee, S. J. (2010). Loss of cofilin 1 disturbs actin dynamics, adhesion between enveloping and deep cell layers and cell movements during gastrulation in zebrafish. *PLoS ONE* **5**,e15331. doi:10.1371/journal.pone.0015331
Lu, P., Vogel, C., Wang, R., Yao, X. and Marcotte, E. M. (2007). Absolute protein expression profiling estimates the relative contributions of transcriptional and translational regulation. *Nat. Biotechnol.* **25**, 117-124. doi:10.1038/nbt1270
Mahaffey, J. P., Grego-Bessa, J., Liem, K. F., Jr. and Anderson, K. V. (2013). Cofilin and Vangl2 cooperate in the initiation of planar cell polarity in the mouse embryo. *Development* **140**, 1262-1271. doi:10.1242/dev.085316
Miyoshi, T. and Watanabe, N. (2013). Can filament treadmilling alone account for the F-actin turnover in lamellipodia? *Cytoskeleton (Hoboken)* **70**, 179-190. doi:10.1002/cm.21098
Moriyama, K. and Yahara, I. (2002). Human CAP1 is a key factor in the recycling of cofilin and actin for rapid actin turnover. *J. Cell Sci.* **115**, 1591-1601. doi:10.1242/jcs.115.8.1591
Nieuwkoop, P. D. and Faber, J. (1994) *Normal Table of Xenopus laevis (Daudin)*. New York: Garland Publishing Inc.
Nolen, B. J., Tomasevic, N., Russell, A., Pierce, D. W., Jia, Z., McCormick, C. D., Hartman, J., Sakowicz, R. and Pollard, T. D. (2009). Characterization of two classes of small molecule inhibitors of Arp2/3 complex. *Nature* **460**, 1031-1034. doi:10.1038/nature08231
Pfister, K., Shook, D. R., Chang, C., Keller, R. and Skoglund, P. (2016). Molecular model for force production and transmission during vertebrate gastrulation. *Development* **143**, 715-727. doi:10.1242/dev.128090
Poukkula, M., Kremneva, E., Serlachius, M. and Lappalainen, P. (2011). Actin-depolymerizing factor homology domain: a conserved fold performing diverse roles in cytoskeletal dynamics. *Cytoskeleton (Hoboken)* **68**, 471-490. doi:10.1002/cm.20530
Püspöki, Z., Storath, M., Sage, D. and Unser, M. (2016). Transforms and operators for directional bioimage analysis: a survey. *Adv. Anat. Embryol. Cell Biol.* **219**, 69-93. doi:10.1007/978-3-319-28549-8_3
Quintero-Monzon, O., Jonasson, E. M., Bertling, E., Talarico, L., Chaudhry, F., Sihvo, M., Lappalainen, P. and Goode, B. L. (2009). Reconstitution and dissection of the 600-kDa Srv2/CAP complex: roles for oligomerization and cofilin-actin binding in driving actin turnover. *J. Biol. Chem.* **284**, 10923-10934. doi:10.1074/jbc.M808760200
Rolland, T., Taşan, M., Charloteaux, B., Pevzner, S. J., Zhong, Q., Sahni, N., Yi, S., Lemmens, I., Fontanillo, C., Mosca, R. et al. (2014). A proteome-scale map of the human interactome network. *Cell.* **159**, 1212-1226. doi:10.1016/j.cell.2014.10.050
Rottner, K. and Schaks, M. (2019). Assembling actin filaments for protrusion. *Curr. Opin. Cell Biol.* **56**, 53-63. doi:10.1016/j.ceb.2018.09.004
Schectman, A. M. (1942). The mechanics of amphibian gastrulation. *Univ. Calif. Pub. Zool* **51**, 1-39.
Shawky, J. H., Balakrishnan, U. L., Stuckenholz, C. and Davidson, L. A. (2018). Multiscale analysis of architecture, cell size and the cell cortex reveals cortical F-actin density and composition are major contributors to mechanical properties during convergent extension. *Development* **145**, dev.161281. doi:10.1242/dev.161281
Shekhar, S. and Carlier, M. F. (2017). Enhanced depolymerization of actin filaments by ADF/Cofilin and monomer funneling by capping protein cooperate to accelerate barbed-end growth. *Curr. Biol.* **27**, 1990-1998.e5. doi:10.1016/j.cub.2017.05.036
Shekhar, S., Chung, J., Kondev, J., Gelles, J. and Goode, B. L. (2019). Synergy between Cyclase-associated protein and Cofilin accelerates actin filament depolymerization by two orders of magnitude. *Nat. Commun.* **10**, 5319. doi:10.1038/s41467-019-13268-1
Shekhar, S., Hoeprich, G. J., Gelles, J. and Goode, B. L. (2021). Twinfilin bypasses assembly conditions and actin filament aging to drive barbed end depolymerization. *J. Cell Biol.* **220**, e202006022. doi:10.1083/jcb.202006022
Shih, J. and Keller, R. (1992a). Cell motility driving mediolateral intercalation in explants of Xenopus laevis. *Development* **116**, 901-914. doi:10.1242/dev.116.4.901
Shih, J. and Keller, R. (1992b). Patterns of cell motility in the organizer and dorsal mesoderm of Xenopus laevis. *Development* **116**, 915-930. doi:10.1242/dev.116.4.915
Shindo, A. (2018). Models of convergent extension during morphogenesis. *Wiley Interdiscip. Rev. Dev. Biol.* **7**, e293. doi:10.1002/wdev.293
Shindo, A. and Wallingford, J. B. (2014). PCP and septins compartmentalize cortical actomyosin to direct collective cell movement. *Science* **343**, 649-652. doi:10.1126/science.1243126
Shindo, A., Inoue, Y., Kinoshita, M. and Wallingford, J. B. (2019). PCP-dependent transcellular regulation of actomyosin oscillation facilitates convergent extension of vertebrate tissue. *Dev. Biol.* **446**, 159-167. doi:10.1016/j.ydbio.2018.12.017
Skoglund, P., Rolo, A., Chen, X., Gumbiner, B. M. and Keller, R. (2008). Convergence and extension at gastrulation require a myosin IIB-dependent cortical actin network. *Development.* **135**, 2435-2444. doi:10.1242/dev.014704
Swaney, K. F. and Li, R. (2016). Function and regulation of the Arp2/3 complex during cell migration in diverse environments. *Curr. Opin. Cell Biol.* **42**, 63-72. doi:10.1016/j.ceb.2016.04.005
Tada, M. and Heisenberg, C. P. (2012). Convergent extension: using collective cell migration and cell intercalation to shape embryos. *Development* **139**, 3897-3904. doi:10.1242/dev.073007
Tahinci, E. and Symes, K. (2003). Distinct functions of Rho and Rac are required for convergent extension during Xenopus gastrulation. *Dev. Biol.* **259**, 318-335. doi:10.1016/S0012-1606(03)00206-9
Tall, E. G., Spector, I., Pentyala, S. N., Bitter, I. and Rebecchi, M. J. (2000). Dynamics of phosphatidylinositol 4,5-bisphosphate in actin-rich structures. *Curr. Biol.* **10**, 743-746. doi:10.1016/S0960-9822(00)00541-8
Theriot, J. A. and Mitchison, T. J. (1991). Actin microfilament dynamics in locomoting cells. *Nature* **352**, 126-131. doi:10.1038/352126a0
Vartiainen, M., Ojala, P. J., Auvinen, P., Peränen, J. and Lappalainen, P. (2000). Mouse A6/twinfilin is an actin monomer-binding protein that localizes to the regions of rapid actin dynamics. *Mol. Cell. Biol.* **20**, 1772-1783. doi:10.1128/MCB.20.5.1772-1783.2000
Wahlström, G., Vartiainen, M., Yamamoto, L., Mattila, P. K., Lappalainen, P. and Heino, T. I. (2001). Twinfilin is required for actin-dependent developmental processes in Drosophila. *J. Cell Biol.* **155**, 787-796. doi:10.1083/jcb.200108022
Walck-Shannon, E., Reiner, D. and Hardin, J. (2015). Polarized Rac-dependent protrusions drive epithelial intercalation in the embryonic epidermis of C. elegans. *Development* **142**, 3549-3560. doi:10.1242/dev.127597
Wallingford, J. B. and Harland, R. M. (2001). Xenopus Dishevelled signaling regulates both neural and mesodermal convergent extension: parallel forces elongating the body axis. *Development* **128**, 2581-2592. doi:10.1242/dev.128.13.2581
Wallingford, J. B., Rowning, B. A., Vogeli, K. M., Rothbacher, U., Fraser, S. E. and Harland, R. M. (2000). Dishevelled controls cell polarity during Xenopus gastrulation. *Nature* **405**, 81-85. doi:10.1038/35011077
Wallingford, J. B., Fraser, S. E. and Harland, R. M. (2002). Convergent extension: the molecular control of polarized cell movement during embryonic development. *Dev. Cell* **2**, 695-706. doi:10.1016/S1534-5807(02)00197-1
Wang, D., Zhang, L., Zhao, G., Wahlström, G., Heino, T. I., Chen, J. and Zhang, Y. Q. (2010). Drosophila twinfilin is required for cell migration and synaptic endocytosis. *J. Cell Sci.* **123**, 1546-1556. doi:10.1242/jcs.060251
Watanabe, N. and Mitchison, T. J. (2002). Single-molecule speckle analysis of actin filament turnover in lamellipodia. *Science* **295**, 1083-1086. doi:10.1126/science.1067470
Weng, S., Huebner, R. J. and Wallingford, J. B. (2021). Convergent extension requires adhesion-dependent biomechanical integration of cell crawling and junction contraction. *bioRxiv*. 2021.2001.2012.426405.
Wilson, P. and Keller, R. (1991). Cell rearrangement during gastrulation of Xenopus: direct observation of cultured explants. *Development* **112**, 289-300. doi:10.1242/dev.112.1.289

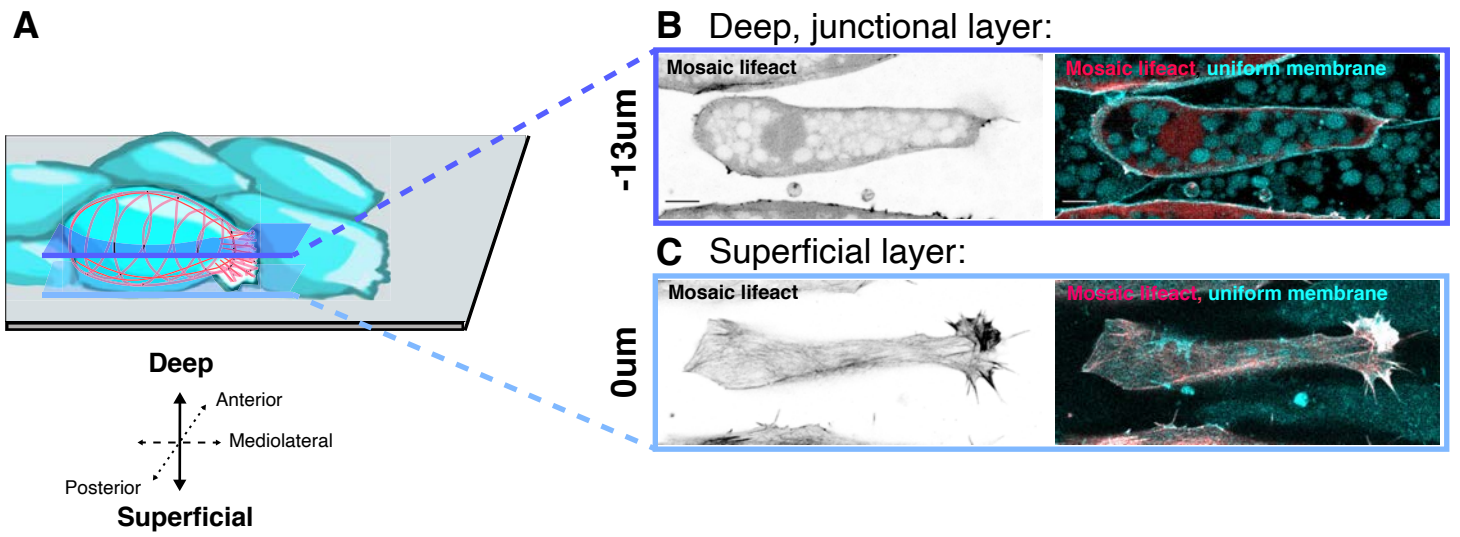

Fig. S1. A) Schematic of dorsal marginal zone explant on a coverslip. **B)** image of deep layer illustrating junctional cortical actin network and small mediolateral protrusion. C) Image of surface cortical actin network and large lamelliform protrusion.

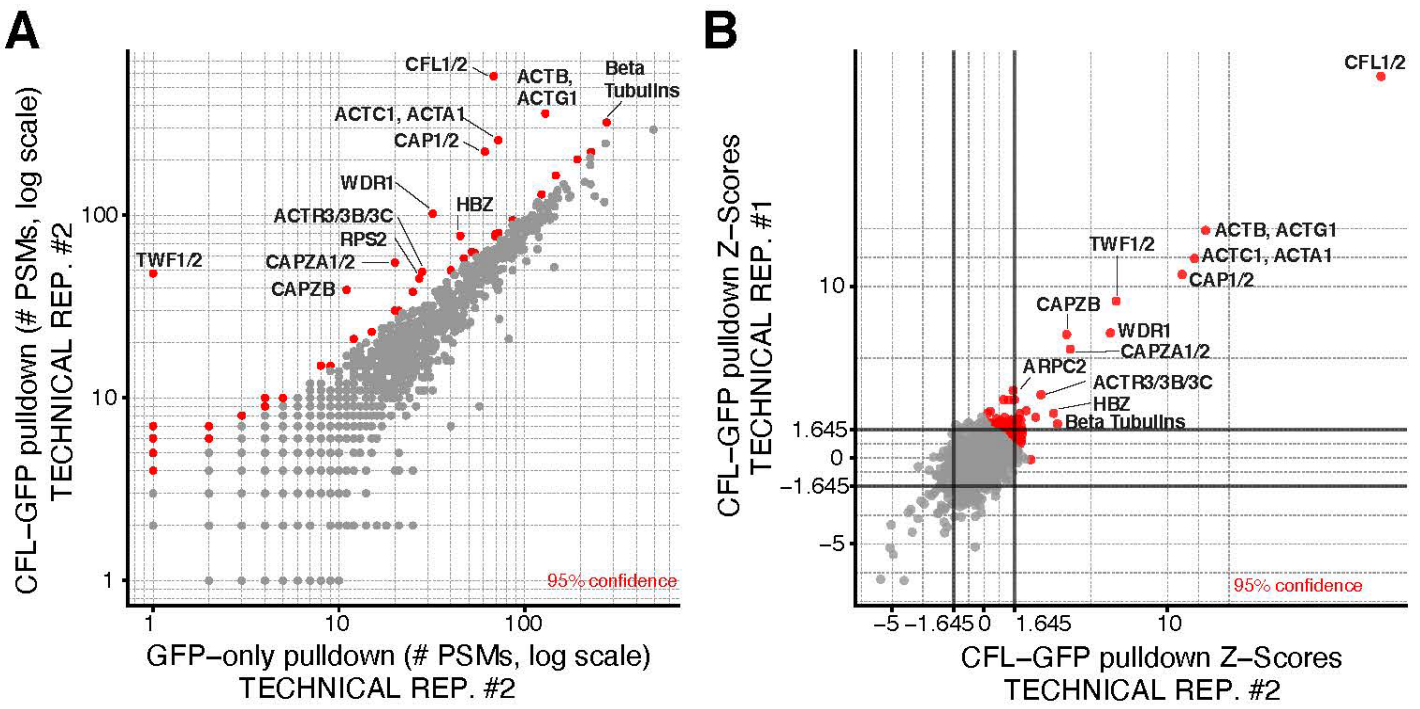

Fig. S2. A) Interaction partners of Cfl2 were identified based on their enrichment in APMS of the Cfl2-GFP-tagged bait protein (vertical axes) relative to APMS of the untagged GFP controls (horizontal axes). Confidence values were calculated by one-sided *Z*-test (see Methods). A pseudocount of 1 PSM was added to each protein for visualization on a log-log plot. **B)** Comparison of technical replicates (A and Fig 2B). Confidence values are based on a joint *Z*-score, calculated by summing the Z-score for each protein in each technical replicate and dividing by the square root of N replicates (*N* = 2).

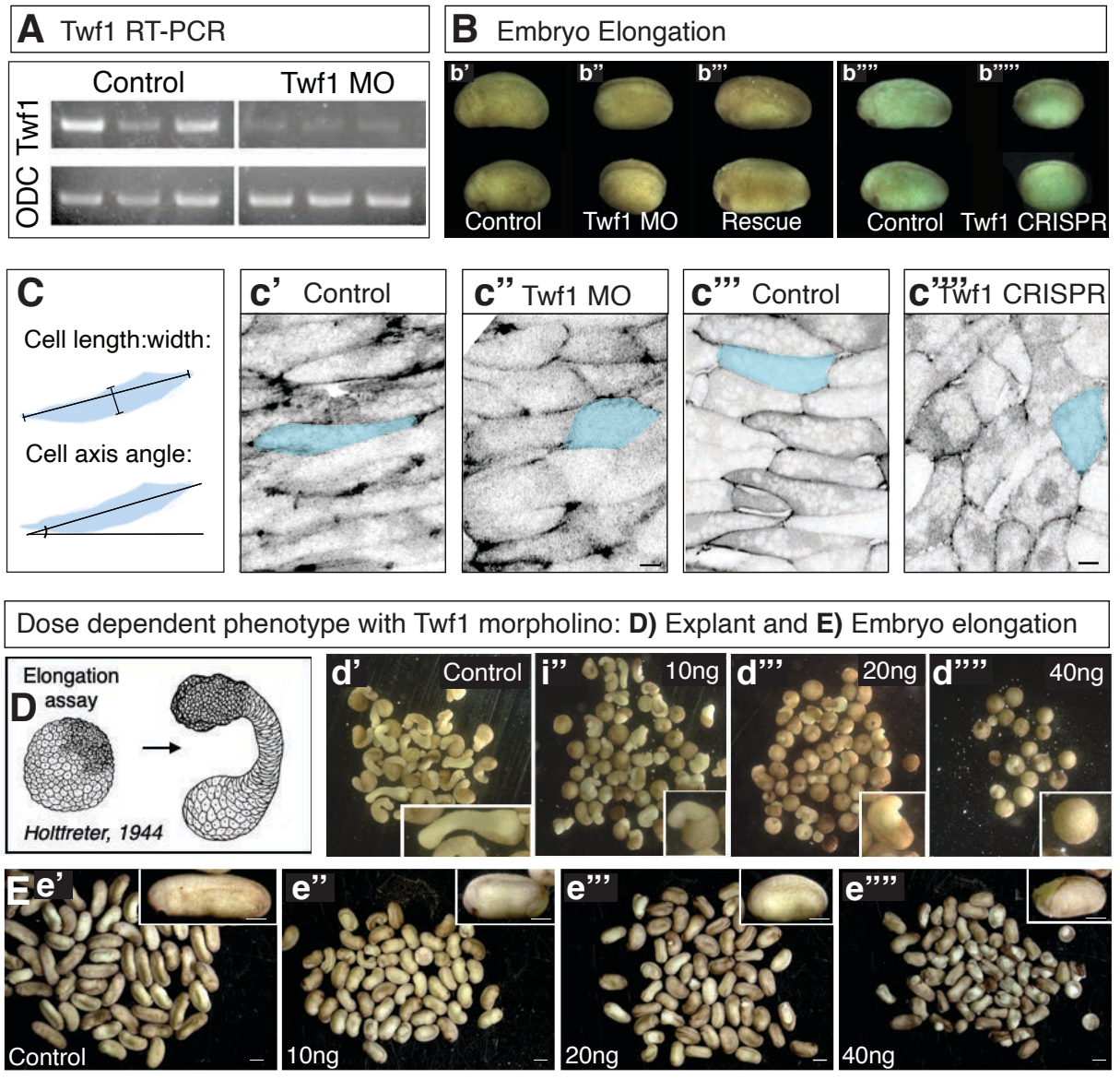

Fig. S3. **A)** RT-PCR showing disruption of Twf1 transcript splicing by the Twf1 MO. **B)** Representative embryos for Twf1 MO-mediated and Twf1 CRISP-mediated knockdown. **C)** Schematic of cell shape (quantified in Fig3C) and cell axis angle quantification along with representative images from control, Twf1 morphant, sgRNA control, and Twf1 crispant cells. **D)** Schematic of DMZ explant elongation assay and explants showing Twf1 morphant DMZs fail to elongate. **E)** Twf1 morphant embryos fail to elongate.

Table S1: Proteomic Data.

Click here to download Table S1

Journal of Cell Science • Supplementary information